Int. J. Electrochem. Sci., 15 **(2020)** 12252 – 12263, doi: 10.20964/2020.12.46

International Journal of
ELECTROCHEMICAL
SCIENCE
www.electrochemsci.org

Promotion of Oxygen Reduction to Hydrogen Peroxide by Ammonium Ions on N-doped Carbon Catalyst

Xiaofeng Wen[1], *Xing Wei*[1], *Gongwei Wang*[1], *Li Xiao*[1,*], *Juntao Lu*[1], *Lin Zhuang*[*, 1, 2]

[1] College of Chemistry and Molecular Sciences, Hubei Key Lab of Electrochemical Power Sources, Wuhan University, Wuhan 430072, China
[2] The Institute for Advanced Studies, Wuhan University, Wuhan 430072, China
[*]E-mail: chem.lily@whu.edu.cn, lzhuang@whu.edu.cn

Received: 2 August 2020 / *Accepted:* 23 September 2020 / *Published:* 31 October 2020

A lot of efforts have been devoted to the improvement of the catalytic activity and hydrogen peroxide (H_2O_2) selectivity of the catalysts in two-electron oxygen reduction reaction (ORR) utilized for production of H_2O_2. Little attention has been paid to the influence of the electrolyte itself. Herein, we report that the two-electron ORR catalytic performance of the catalyst strongly depends on the cations of the electrolyte. The catalytic performance of an N-doped carbon (PNC) catalyst has been evaluated in two different aqueous electrolytes: $(NH_4)_2SO_4$ and Na_2SO_4. The results show that the ORR catalytic activity and the H_2O_2 selectivity in $(NH_4)_2SO_4$ solution are much better than that in Na_2SO_4 solution, namely with H_2O_2 FE of 90.2% and current density of 13.9 mA cm^{-2} in $(NH_4)_2SO_4$ compared to 67.8% and 2.5 mA cm^{-2} in Na_2SO_4. The *in-situ* Fourier transform infrared (FTIR) spectroscopy shows that H_2O acts in the reaction in Na_2SO_4 solution as a proton source, but there was no evidence of the same role of H_2O in $(NH_4)_2SO_4$ solution. Further experimental results also show that the ORR performance of PNC is dependent on the concentration of $(NH_4)_2SO_4$ solution, but independent on the concentration of Na_2SO_4 solution. Thus, we reasonably infer that ammonium ions have promoted the ORR catalytic performance of PNC.

Keywords: oxygen reduction reaction, hydrogen peroxide, faradaic efficiency, electrocatalysis, ATR-FTIR

1. INTRODUCTION

H_2O_2 is widely used in various fields: as disinfector in medicine, as green chemical oxidant and as industrial wastewater treatment agent [1-3]. Currently, H_2O_2 is mainly produced by industrial anthraquinone indirect synthesis method [4]. However, there are still serious challenges in this process such as generation of large amount of industrial waste, high storage and transportation costs [5]. An alternative approach is direct H_2O_2 synthesis from H_2 and O_2 [6-8]. However, the explosion risk in case

of mixing H_2 and O_2, as well as the necessity of noble metal catalysts usage, limiting the large-scale application of this method [9, 10]. Therefore, researchers are still searching for alternative methods for H_2O_2 production with high efficiency, low cost and high safety [11].

The two-electron electrochemical oxygen reduction reaction (ORR) is a desirable approach for H_2O_2 preparation, allowing to avoid the abovementioned disadvantages of direct and indirect synthesis methods [12,13]. The electrochemical approach can be carried out at normal temperature and pressure, which is safer and more convenient for operation, and can be powered by environment-friendly renewable energy [14]. The electrochemical ORR to H_2O_2 on non-precious carbon materials demonstrated high selectivity with a relatively low overpotential in alkaline media [11, 15]. However, H_2O_2 is extremely unstable in alkaline media [16], and the overpotential of the two-electron ORR is relative high in acidic media. Therefore, it is desired to produce H_2O_2 in a pH neutral solution [17].

Previous studies of the two-electron ORR mainly focused on the electrocatalytic materials (e.g. N-doped carbons) or active sites, whereas rare reports demonstrated the impact of the electrolytes with K_2SO_4 as the most commonly used neutral electrolyte with phosphate buffer solution [11, 18]. The reported results of high H_2O_2 Faraday efficiency (FE) are always accompanied with low current density. Therefore, it is still a challenge for non-precious catalysts in neutral electrolyte to simultaneously obtain a high H_2O_2 selectivity and high catalytic activity towards the two-electron ORR.

In this work, we explore the electrocatalytic activity and H_2O_2 selectivity of a protein derived N-doped carbon (denoted as PNC) catalyst in two different neutral electrolytes: Na_2SO_4 and $(NH_4)_2SO_4$ solution, and report a superior H_2O_2 FE of 90.2% with high current density of 13.9 mA cm^{-2} in $(NH_4)_2SO_4$ solution. The *in-situ* FTIR spectroscopy characterization indicated that the direct proton source of ORR in Na_2SO_4 comes from H_2O, while the presence of ammonium ions may affect the proton transfer pathway of ORR.

2. EXPERIMENTAL SECTION

2.1 Synthesis of protein derived nitrogen-doped carbon (PNC)

Egg white (30 mL, approximately the amount from one egg) was added to ultrapure water (18.25 MΩ·cm, 10 mL), and then mixed under magnetic stirring at 40^{o}C until a transparent solution formed. 1 g of $4MgCO_3 \cdot Mg(OH)_2 \cdot 5H_2O$ was added to the protein solution, and then ultrasonically blended for 20 min after magnetic stirring for 3.5 h. A solid product was collected by centrifugation, then freeze dried under vacuum. Then the solid product was grounded to fine powders by mortar, and annealed in a tubular furnace at 600^{o}C for 2 hours (heating rate: 5^{o}C min^{-1}) under Ar atmosphere. After the pyrolysis, MgO was removed in 1.5 M HCl. The carbon material was washed 5 times with ultrapure water and freeze dried under vacuum before usage. All chemicals are analytical grade and purchased from Sinopharm Chemical Reagent Co., China.

2.2 Material characterization

Scanning electron microscope (SEM) characterization was performed by using a Zeiss Merlin Compact microscope at acceleration voltage of 5 kV. XPS studies were conducted on a Thermo Fisher EscaLab 250Xi spectrometer with Al Kα source (hv = 1486.6 eV). The N-1s spectra was analyzed and processed by XPSPEAK41 software.

2.3 Electrochemical performance measurements

5 mg of catalysts was added to 1 mL of Nafion alcohol solution (0.05 wt%), and then ultrasonically blended for 0.5 h to form uniform ink. 10 μL of the obtained ink was dropped onto a rotating ring-disk electrode (RRDE, ϕ = 4.57 mm, Pine Inc.) with a syringe. The coating catalyst was dried under infrared light. A rectangular carbon paper was used as the counter electrode, and an Hg/Hg_2SO_4 electrode was used as the reference electrode. All potentials were converted to the reversible hydrogen electrode (RHE). Electrochemical tests were performed on a CHI-700A Bi-Potentiostat. 1 M $(NH_4)_2SO_4$ (pH=5.5) and 1 M Na_2SO_4 (pH=6) aqueous solution were separately used as electrolyte. The RRDE test was conducted in a standard 5-port electrolytic cell at 25°C. The polarization curves were recorded between 0.05 V vs. RHE and 0.85 V vs. RHE at 5 mV s^{-1} at 1600 rpm and 1.2 V vs. RHE was applied on the Pt ring electrode in the RRDE tests. The collection efficiency of the RRDE was 0.22. The selectivity for H_2O_2 formation (H_2O_2%) and the number of transferred electrons (n) were calculated using the ring and disk currents and the collection efficiency [18].

2.4 Production of H_2O_2 by electrolysis

The aforementioned ink was pipetted onto both sides of a carbon paper with an area of 7×7 mm and utilized as the working electrode after drying. The bulk electrolysis was performed using H-type electrolytic cell separated by Nafion membrane (Figure S1). The three-electrode system was consisted of an Hg/Hg_2SO_4 electrode as a reference electrode, a Pt sheet as a counter electrode and the working electrode. 10 mL of O_2-saturated $(NH_4)_2SO_4$ solution or Na_2SO_4 solution was used as electrolyte.

Bulk H_2O_2 production was obtained by chronoamperometry at 0.0-0.3 V vs. RHE for 10 min. The H_2O_2 concentration was measured using UV-vis spectroscopy calibration curve method. To obtain the calibration curve, a series of H_2O_2 solutions with gradient concentrations were added to 1 ml of 3 M H_2SO_4 and 1 ml of 0.05 M $C_4K_2O_9{\cdot}2H_2O$ solution and measured by UV-vis spectroscopy [19]. After the electrolysis, 4 mL of electrolyte was taken from the cathode compartment, and then 1 ml of 3 M H_2SO_4 and 1 ml of 0.05 M $C_4K_2O_9{\cdot}2H_2O$ solution were added before the UV-vis measurement. Based on the linear relationship between the UV-vis intensity and H_2O_2 concentration (10 ~ 40 mM), the H_2O_2 concentrations of the samples could be obtained (Figure S2). The H_2O_2 FE was calculated from the actual H_2O_2 product against the quantity of charge passed [20]. The current density of H_2O_2 (j_{H2O2}) was calculated by the following equation:

$$j_{H_2O_2} = j_{ORR} \times H_2O_2\ \mathrm{FE}\ (\%), \quad (1)$$

where j_{ORR} is total reaction current density (mA/cm^2).

2.5 In situ ATR-FTIR study

To enhance the infrared signal, an Au nanofilm was deposited by a secondary chemical gilding method on a Si prism [21]. The aforementioned ink was then dropped onto the Au nanofilm and utilized as the working electrode after drying. The IR beam passed through the electrode interface by reflection (Figure S3). The *in-situ* attenuated total reflection surface-enhanced IR absorption spectroscopy (ATR-SEIRAS) study was conducted using a Thermo Fisher Nicolet 6700 spectrometer with an MCT detector with resolution of 16 cm^{-1} and a total of 32 interferograms. All infrared spectra ordinates were expressed in absorbance (A). The infrared spectra at 0.7 V vs. RHE under Ar atmosphere were used as the background. The infrared spectra were collected while performing chronoamperometry at 0.6-0.0 V vs. RHE.

3. RESULTS AND DISCUSSION

3.1 Activity and selectivity in different electrolytes

Carbon materials are widely used in the field of electrocatalysis because of their large surface area and good conductivity, whereas nitrogen doping was reported as a feasible way for further improvement of the catalytic activity and the H_2O_2 selectivity of carbon materials [22, 23]. The PNC catalyst was synthesized by the template method and according to the SEM characterization, the PNC catalyst was obtained in the form of nanoflakes (Figure S4). XPS characterization was used to identify the various N-species in the PNC. Figure S5 displays the N-1s core level XPS spectra, which could be fitted with four distinct peaks, classified as pyridinic-N (398.4 eV), pyrrolic-N (399.9 eV), quaternary-N (400.7 eV), and graphitic-N (402.5 eV), respectively [24, 25].

The ORR catalytic performance of PNC was evaluated in Na_2SO_4 and $(NH_4)_2SO_4$ solutions with various concentrations. Figure 1(a, b) shows the current density of H_2O_2 production and the side reactions at different applied potentials from 0.0 to 0.3 V vs. RHE. Overall, the current density of H_2O_2 and the H_2O_2 FE in $(NH_4)_2SO_4$ solution (Figure 1(b)) was much higher than that in Na_2SO_4 solution (Figure 1(a)) in the investigated potential range. The current density of H_2O_2 was lower than 2 mA/cm^2 in all Na_2SO_4 solutions, but could reach as high as 12.5 mA/cm^2 in $(NH_4)_2SO_4$ solution. Meanwhile, the current density of H_2O_2 was independent on the Na_2SO_4 concentration (Figure 1(a)). In contrast, the current density of H_2O_2 and the H_2O_2 FE increased with the increase of $(NH_4)_2SO_4$ concentration at 0.0 V vs. RHE (Figure 1(b)). Solutions exhibiting best catalytic performance, namely1 M $(NH_4)_2SO_4$ and 1 M Na_2SO_4, were further compared in Figure 1(c) and 1(d). 1 M $(NH_4)_2SO_4$ solution attributed to the highest H_2O_2 FE of 90.2% at 0.0 V vs. RHE, which was comparable to the results of the reported non-precious catalysts, while the current density of 13.9 mA/cm^2 is much higher than that reported in the literature (Table S1**)**. It is worth noting that the H_2O_2 FE and the current density in 1 M $(NH_4)_2SO_4$ solution were 1.33 and 5.56 times higher than that in 1 M Na_2SO_4 solution respectively.

It is well known that the ORR catalytic activity and the H_2O_2 FE are sensitive to pH of the solution [17]. Therefore, in the abovementioned experiments, one might doubt that higher catalytic

performance for H_2O_2 generation resulted from lower pH of $(NH_4)_2SO_4$ solution. To eliminate this doubt, a certain amount of H_2SO_4 solution was added to 1 M Na_2SO_4 solution to adjust the pH from 6.0 to 5.5, which was the same as the pH of 1 M $(NH_4)_2SO_4$ solution.

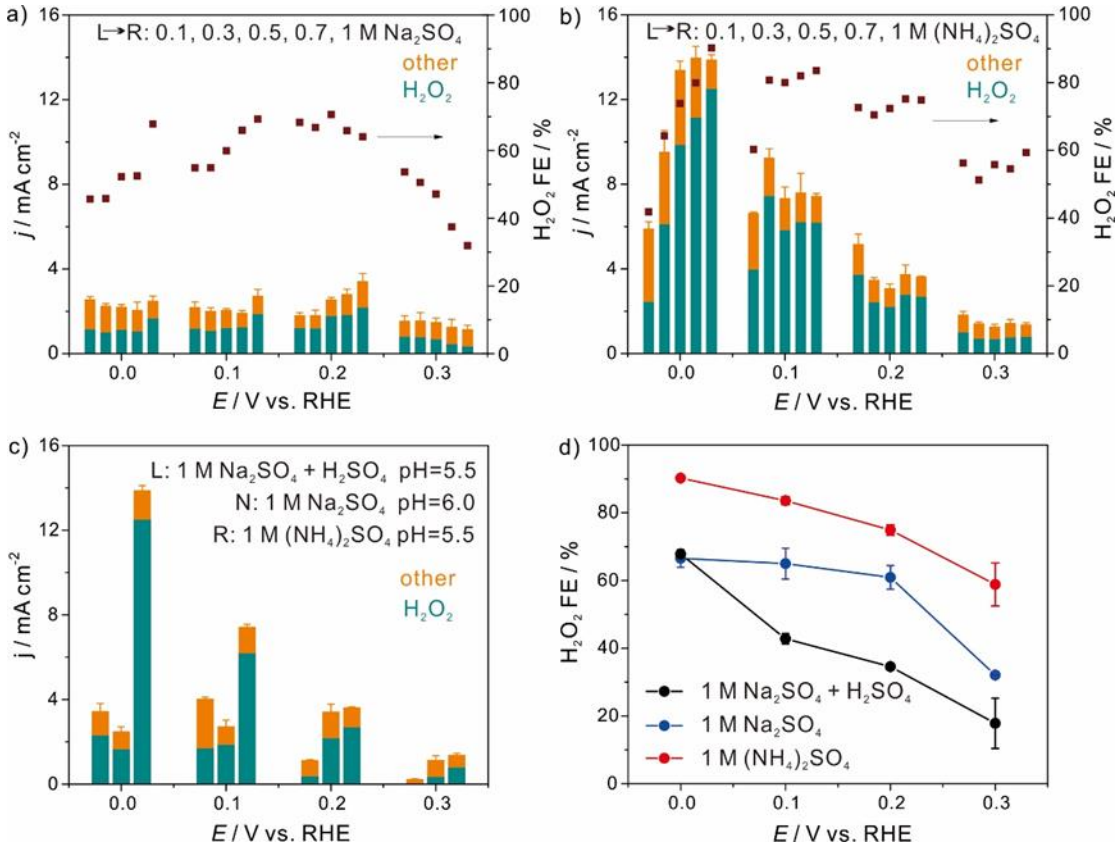

Figure 1. Current density of H_2O_2 and side reaction and H_2O_2 Faraday efficiency (FE) in O_2-saturated 0.1, 0.3, 0.5, 0.7, 1 M Na_2SO_4 (a), 0.1, 0.3, 0.5, 0.7, 1 M $(NH_4)_2SO_4$ (b) solutions. Current density of H_2O_2 and side reaction in O_2-saturated 1 M Na_2SO_4 and H_2SO_4 (pH=5.5), 1 M Na_2SO_4 (pH=6.0) and1 M $(NH_4)_2SO_4$ (pH=5.5) (c). The H_2O_2 FE in O_2-saturated 1 M Na_2SO_4 and H_2SO_4 (pH=5.5), 1 M Na_2SO_4 (pH=6.0) and 1 M $(NH_4)_2SO_4$ (pH=5.5) (d).

As shown in Figure 1(c) and 1(d), the change of pH from 6.0 to 5.5 did not strongly affect the H_2O_2 current density and the H_2O_2 FE in Na_2SO_4 solution, indicating that the reason for higher ORR catalytic performance in $(NH_4)_2SO_4$ solution was not pH.

3.2 Overall electron transfer

The electrocatalytic activity and selectivity of PNC towards ORR in 1 M Na_2SO_4 and 1 M $(NH_4)_2SO_4$ solutions were further examined by the RRDE method. Figure 2(a), 2(c) shows the experimental results in 1 M Na_2SO_4 and 1 M $(NH_4)_2SO_4$ solutions. The ORR current density was measured on the disk electrode and the H_2O_2 oxidation current was measured on the Pt ring electrode. According to the polarization curves, the ORR onset potential shifted positively from 0.52 V in 1 M Na_2SO_4 solution to 0.63 V in 1 M $(NH_4)_2SO_4$ solution, and the current was obviously higher in 1 M

$(NH_4)_2SO_4$. The H_2O_2% and number of transferred electrons were also derived from the RRDE polarization curves (Figure 2(b), 2(d)).

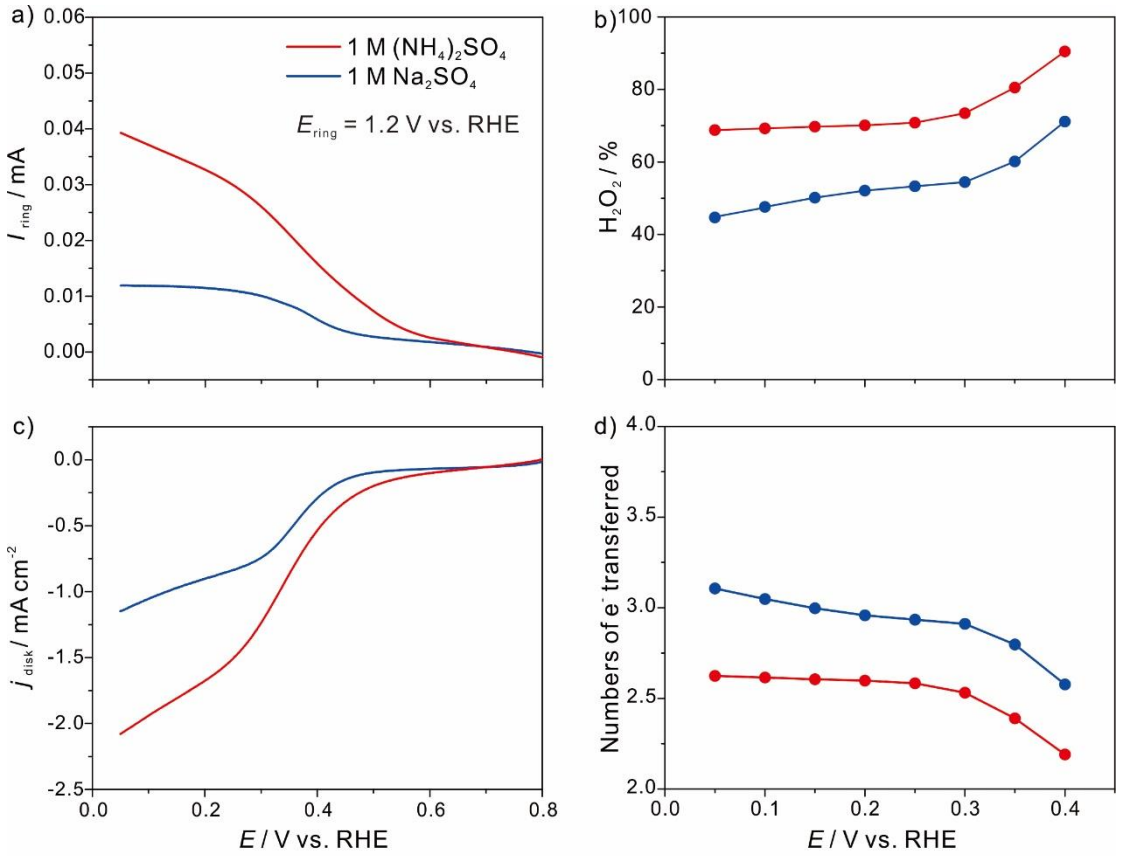

Figure 2. Linear sweep voltammetry of RRDE with the ring current (a), disk geometric current density (c), H_2O_2 selectivity (b) number of transferred electrons (n) as a function of PNC electrode potential (d). Conditions: the catalyst loading amount on the disk electrode was set to be 0.3 mg cm^{-2}, and measurements were performed in O_2-saturated 1 M Na_2SO_4 and 1 M $(NH_4)_2SO_4$ at a scan rate of 5 mV/s with 1600 rpm at 25°C.

The H_2O_2% in 1 M $(NH_4)_2SO_4$ solution reached ~90% at 0.4 V, in comparison to ~70% in Na_2SO_4 solution, and the electron transfer number in 1 M $(NH_4)_2SO_4$ solution was around ~2.2, in comparison with ~2.6 in Na_2SO_4 solution. On the basis of RRDE results, it can be concluded that the PNC performed better in 1 M $(NH_4)_2SO_4$ solution than in 1 M Na_2SO_4 solution, which is in consistence with the conclusion, drawn from the first discussion section.

3.3 In Situ FTIR observations

In situ ATR-SEIRAS was used to explore the ORR process in 1 M Na_2SO_4 and $(NH_4)_2SO_4$ solution [26]. The SEIRAS spectra on PNC surfaces were obtained in the potential range from 0.6 V to

0.0 V vs. RHE. Figure 3(a) and 3(b) are the real-time infrared spectra for ORR in 1 M Na_2SO_4 solution in Ar and O_2 atmosphere, respectively.

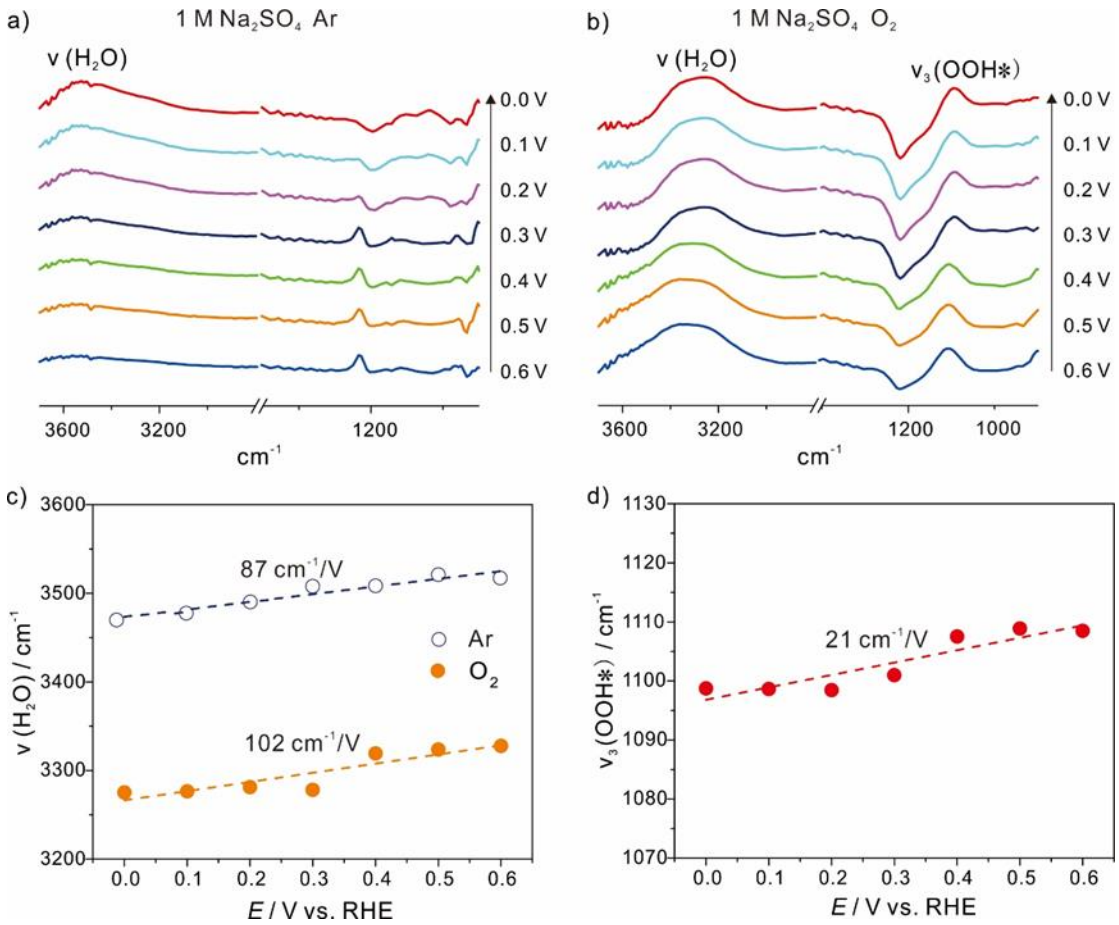

Figure 3. SEIRAS spectra recorded in: 1 M Na_2SO_4 solution Ar-saturated (a) and O_2-saturated (b). Stark effects of the linearly adsorbed: H_2O in Ar/O_2-saturated 1 M Na_2SO_4 (c), OOH* in O_2-saturated 1 M Na_2SO_4 (d). The reference spectrum was taken at 0.7 V in Ar-saturated solution.

In the obtained SEIRAS spectra there were detected two vital bands at 3600-3000 cm^{-1} and 1200-1000 cm^{-1}, which can be classified as the stretching of adsorbed H_2O and OOH*, respectively [27, 28]. Specifically, the H_2O stretching vibration, ν(HOH), appeared at a lower wavenumbers in O_2 than in Ar atmosphere, with Stark effects of ν(HOH) stronger in O_2 than in Ar atmosphere (Figure 3(c)), indicating a stronger PNC-H_2O interaction during ORR in 1 M Na_2SO_4 solution [26, 27]. In addition, the intensity of H_2O adsorbed at O_2 atmosphere was ~11 times higher than that in Ar atmosphere (Figure S7(a)), indicating a high coverage of H_2O on the electrode surface in 1 M Na_2SO_4 solution during ORR. These are clear evidences for H_2O participated in the ORR in 1 M Na_2SO_4 solution. Moreover, OOH* is regarded as an important intermediate for generating H_2O_2 in the ORR [17, 29]. As shown in Figure 3(b), the OOH* band turned out to be at 1100 cm^{-1} in 1 M Na_2SO_4 solution in O_2 atmosphere. The Stark effect of ν_3(OOH*) (wavenumber shift with potential, Figure 3(d)) suggests that OOH* is an adsorbed intermediate for ORR in 1 M Na_2SO_4 solution [30].

In contrast, no H_2O stretching vibration bands were observed in 1 M $(NH_4)_2SO_4$ solution (Figure 4(a), 4(b)), indicating that the signal of H_2O_{ads} in this condition was almost the same with the background and the reaction process related to the surface water might change in $(NH_4)_2SO_4$ solution. However, the infrared stretch vibration of surface H_2O is in the wave number range of 3600-3000 cm^{-1} and the infrared signal of NH_4^+ is weak and registered at 3200-3000 cm^{-1} [31]. Therefore, it is unable to obtain the infrared signal of NH_4^+ due to the interference with the surface H_2O. In addition, no OOH* band was observed in 1 M $(NH_4)_2SO_4$ solution (Figure 4(b)), indicating that protonation was too rapid in $(NH_4)_2SO_4$ solution to detect the intermediates.

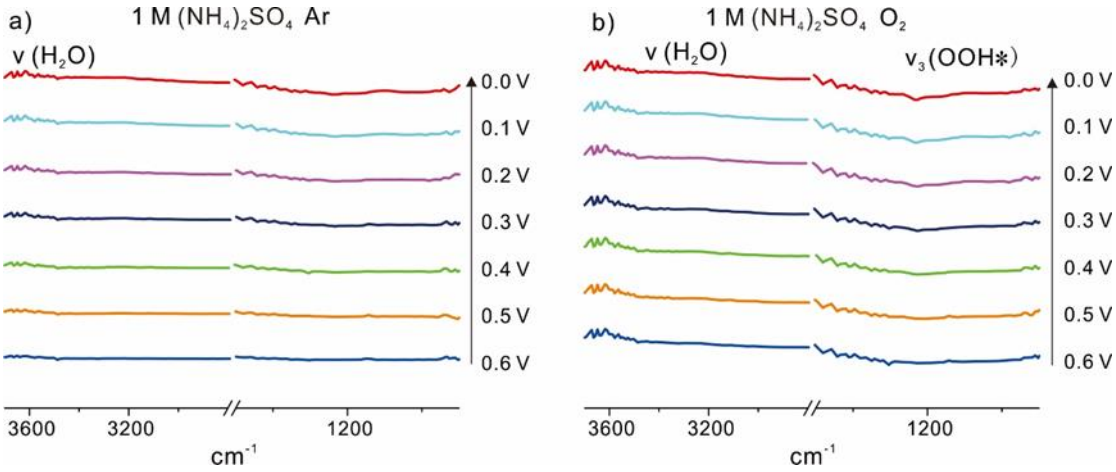

Figure 4. SEIRAS spectra recorded in: 1 M $(NH_4)_2SO_4$ solution Ar-saturated (a) and O_2-saturated (b). The reference spectrum was taken at 0.7 V in Ar-saturated solution.

In the two-electron ORR, the adsorbed O_2 continuously consumes protons and electrons to generate H_2O_2 (Eq. 2, 3) [32].

$$* + O_2 + H^+ + e^- = OOH* \quad (2)$$

$$OOH* + H^+ + e^- = H_2O_2 + * \quad (3)$$

Where the asterisk (*) represent the catalyst active site. Clearly, the proton transfer process is as crucial as over-potential in these reactions. Based on SEIRAS experiments, it is clear that protons were provided by H_2O in Na_2SO_4 solution in Eq. 2 and 3. In contrast, no surface H_2O-related reaction evidence was provided by SEIRAS in $(NH_4)_2SO_4$ solution. Combining with the concentration dependency relationship between the $(NH_4)_2SO_4$ solution and the H_2O_2 catalytic activity/selectivity, it can be reasonably inferred that the two-electron ORR was affected by the NH_4^+ concentration.

4. CONCLUSION

In this paper, we observed that the two-electron ORR catalytic activity and H_2O_2 FE of PNC were significantly improved in $(NH_4)_2SO_4$ solution, in comparison to those in Na_2SO_4 solution. The H_2O_2 FE increased from 67.8% (in 1 M Na_2SO_4 solution) to 90.2% (in 1 M $(NH_4)_2SO_4$ solution) at 0.0 V vs. RHE. Moreover, according to the *in situ* electrochemical SEIRAS measurement, the surface H_2O

directly participated in the ORR in Na_2SO_4 solution, but no surface H_2O-related reaction evidence was found in $(NH_4)_2SO_4$ solution. Considering the facts that the two-electron ORR catalytic activity and H_2O_2 FE of PNC were dependent on the concentration of $(NH_4)_2SO_4$ solution but independent on the concentration of Na_2SO_4 solution, we can reasonably propose that the H_2O_2 production catalytic performance of PNC was improved due to presence of NH_4^+ ions.

This work provides a new perspective to improve the FE and yield of H_2O_2 of the catalysts through an electrolyte point of view.

ACKNOWLEDGMENTS

This work was supported by the National Natural Science Foundation of China (21872108, 21633008 and 40891545205), Wuhan University Innovation Team (2042017kf0232), the National Key Research and Development Program (2016YFB0101203) and the Fundamental Research Funds for the Central Universities (2042020kf1073)

References

1. S. Yang, A. Verdaguer-Casadevall, L. Arnarson, L. Silvio, V. Colic, R. Frydendal, J. Rossmeisl, I. Chorkendorff, I. E. L. Stephens, *Acs Catal.*, 8 (2018) 4064.
2. I. Yamanaka, T. Murayama, *Angew. Chem. Int. Edit.*, 47 (2008) 1900.
3. E. Brillas, I. Sires, M. A. Oturan, *Chem. Rev.*, 109 (2009) 6570.
4. J. M. Campos-Martin, G. Blanco-Brieva, J. L. G. Fierro, *Angew. Chem. Int. Edit.*, 45 (2006) 6962.
5. B. Puertolas, A. K. Hill, T. Garcia, B. Solsona, L. Torrente-Murciano, *Catal. Today*, 248 (2015) 115.
6. R. Arrigo, M. E. Schuster, S. Abate, G. Giorgianni, G. Centi, S. Perathoner, S. Wrabetz, V. Pfeifer, M. Antonietti, R. Schloegl, *Acs Catal.*, 6 (2016) 6959.
7. S. Maity, M. Eswaramoorthy, *J. Mater Chem A*, 4 (2016) 3233.
8. N. M. Wilson, D. W. Flaherty, *J. Am. Chem. Soc.*, 138 (2016) 574.
9. J. K. Edwards, B. Solsona, E. N. N, A. F. Carley, A. A. Herzing, C. J. Kiely, G. J. Hutchings, *Science*, 323 (2009) 1037.
10. S. J. Freakley, Q. He, J. H. Harrhy, L. Lu, D. A. Crole, D. J. Morgan, E. N. Ntainjua, J. K. Edwards, A. F. Carley, A. Y. Borisevich, C. J. Kiely, G. J. Hutchings, *Science*, 351 (2016) 965.
11. Z. Lu, G. Chen, S. Siahrostami, Z. Chen, K. Liu, J. Xie, L. Liao, T. Wu, D. Lin, Y. Liu, T. F. Jaramillo, J. K. Norskov, Y. Cui, *Nature Catalysis*, 1 (2018) 156.
12. C. Xia, Y. Xia, P. Zhu, L. Fan, H. Wang, *Science*, 366 (2019) 226.
13. W. P. I. Mounfield, A. Garg, Y. Shao-Horn, Y. Roman-Leshkov, *Chem-Us*, 4 (2018) 18.
14. Z. Chen, S. Chen, S. Siahrostami, P. Chakthranont, C. Hahn, D. Nordlund, S. Dimosthenis, J. K. Norskov, Z. Bao, T. F. Jaramillo, *React Chem Eng.*, 2 (2017) 239.
15. V. Colic, S. Yang, Z. Revay, I. E. L. Stephens, I. Chorkendorff, *Electrochim. Acta*, 272 (2018) 192.
16. J. Gao, H. B. Yang, X. Huang, S. Hung, W. Cai, C. Jia, S. Miao, H. M. Chen, X. Yang, Y. Huang, T. Zhang, B. Liu, *Chem-Us*, 6 (2020) 658.
17. Y. Jiang, P. Ni, C. Chen, Y. Lu, P. Yang, B. Kong, A. Fisher, X. Wang, *Adv Energy Mater*, 8 (2018).
18. Y. Sun, I. Sinev, W. Ju, A. Bergmann, S. Dresp, S. Kuehl, C. Spoeri, H. Schmies, H. Wang, D. Bernsmeier, B. Paul, R. Schmack, R. Kraehnert, B. Roldan Cuenya, P. Strasser, *Acs Catal.*, 8 (2018) 2844.

19. Y. Sheng, S. Song, X. Wang, L. Song, C. Wang, H. Sun, X. Niu, *Electrochim. Acta*, 56 (2011) 8651.
20. Y. Liu, X. Quan, X. Fan, H. Wang, S. Chen, *Angew. Chem. Int. Edit.*, 54 (2015) 6837.
21. X. Xue, J. Wang, Q. Li, Y. Yan, J. Liu, W. Cai, *Anal. Chem.*, 80 (2008) 166.
22. T. Fellinger, F. Hasche, P. Strasser, M. Antonietti, *J. Am. Chem. Soc.*, 134 (2012) 4072.
23. D. Iglesias, A. Giuliani, M. Melchionna, S. Marchesan, A. Criado, L. Nasi, M. Bevilacqua, C. Tavagnacco, F. Vizza, M. Prato, P. Fornasiero, *Chem-Us*, 4 (2018) 106.
24. Y. Nie, L. Li, Z. Wei, *Chem. Soc. Rev.*, 44 (2015) 2168.
25. Z. Li, Z. Xu, X. Tan, H. Wang, C. M. B. Holt, T. Stephenson, B. C. Olsen, D. Mitlin, *Energ Environ Sci.*, 6 (2013) 871.
26. Y. Wang, Y. Yang, S. Jia, X. Wang, K. Lyu, Y. Peng, H. Zheng, X. Wei, H. Ren, L. Xiao, J. Wang, D. A. Muller, H. D. Abruna, B. J. Hwang, J. Lu, L. Zhuang, *Nat Commun.*, 10 (2019).
27. X. Wei, Z. Yin, K. Lyu, Z. Li, J. Gong, G. Wang, L. Xiao, J. Lu, L. Zhuang, *Acs Catal.*, 10 (2020) 4103.
28. K. Kunimatsu, T. Yoda, D. A. Tryk, H. Uchida, M. Watanabe, *Phys. Chem. Chem. Phys.*, 12 (2010) 621.
29. S. Siahrostami, A. Verdaguer-Casadevall, M. Karamad, D. Deiana, P. Malacrida, B. Wickman, M. Escudero-Escribano, E. A. Paoli, R. Frydendal, T. W. Hansen, I. Chorkendorff, I. E. L. Stephens, J. Rossmeisl, *Nat. Mater.*, 12 (2013) 1137.
30. D. K. Lambert, *Electrochim. Acta*, 41 (1996) 623.
31. C. Costentin, M. Robert, J. Saveant, *J. Phys Chem C.*, 111 (2007) 12877.
32. S. Fukuzumi, Y. Lee, W. Nam, *Chemcatchem*, 10 (2018) 9.

SUPPLEMENTARY DATA:

Table S1. Comparison of reaction current density and H_2O_2 Faraday efficiency in the H-type electrolytic cell in aqueous media.

Catalyst	Working media	Current density (mA cm^{-2})	Potential (V vs. RHE)	H_2O_2FE (%)	Ref.
N-doped carbon	1 M $(NH_4)_2SO_4$	13.9	0.0	90.2	This work
N-doped carbon	1 M Na_2SO_4	2.5	0.0	67.8	This work
YP-80F	0.1M HClO4	~3	-0.2	82	15
BP-2000	0.1M $HClO_4$	~2~	-0.2	82	15
N-doped carbon	0.5 M H_2SO_4	~0.2	0.3	~90	18
N-doped carbon	0.1 M K2SO4	~3.5	0.2	~75	18
N-doped carbon	0.1 M PBS	~0.5	-	~90	23

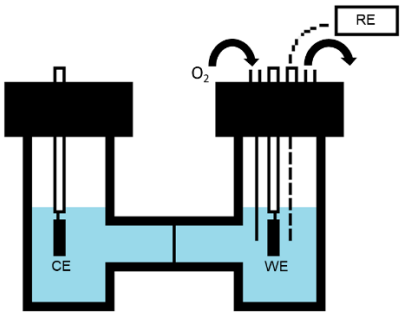

Figure S1. Schematic diagram of the H-type electrolytic cell.

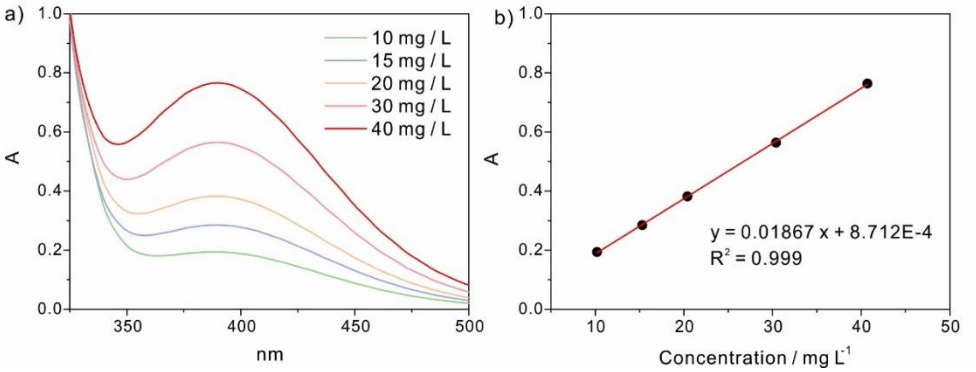

Figure S2. (a) Ultraviolet spectrum with a scanning range of 300-500 nm. (b) Ultraviolet standard curve.

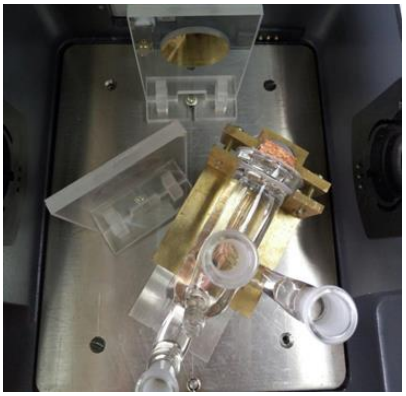

Figure S3. Figure of electrolytic cell for ATR-SEIRAS.

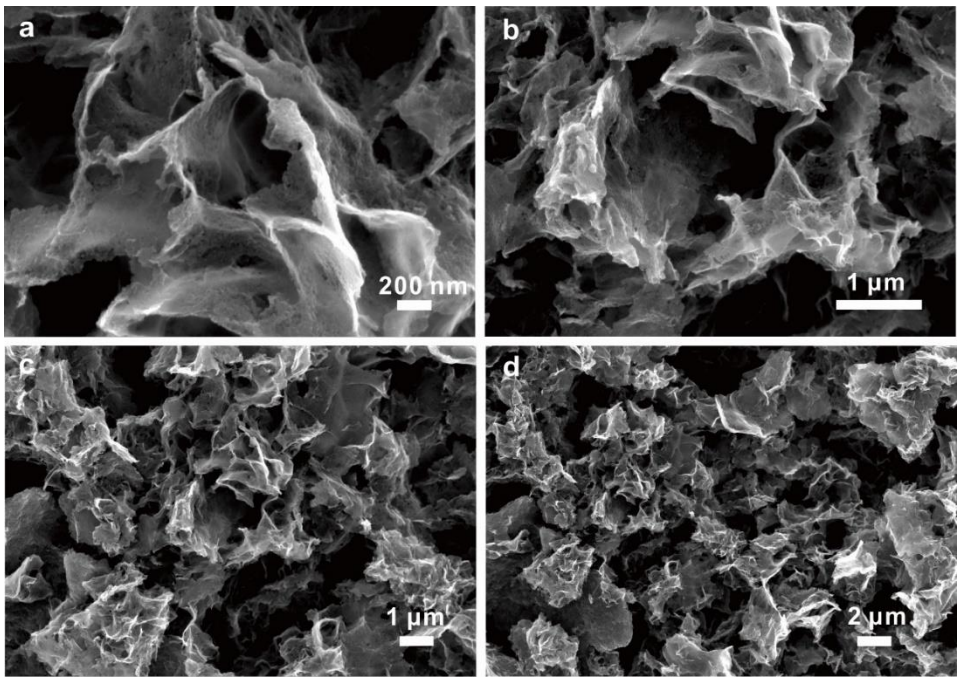

Figure S4. SEM images of PNC. Scale bars = 200 nm (a); 1 μm (b, c); 2 μm (d).

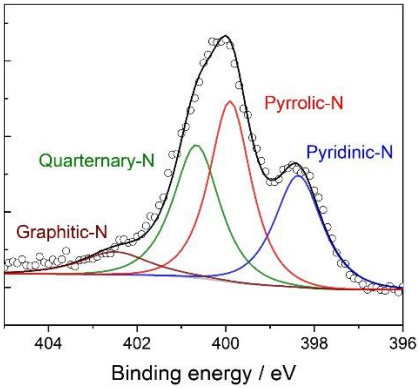

Figure S5. XPS spectra of the N-1s core level region of N-doped carbon.

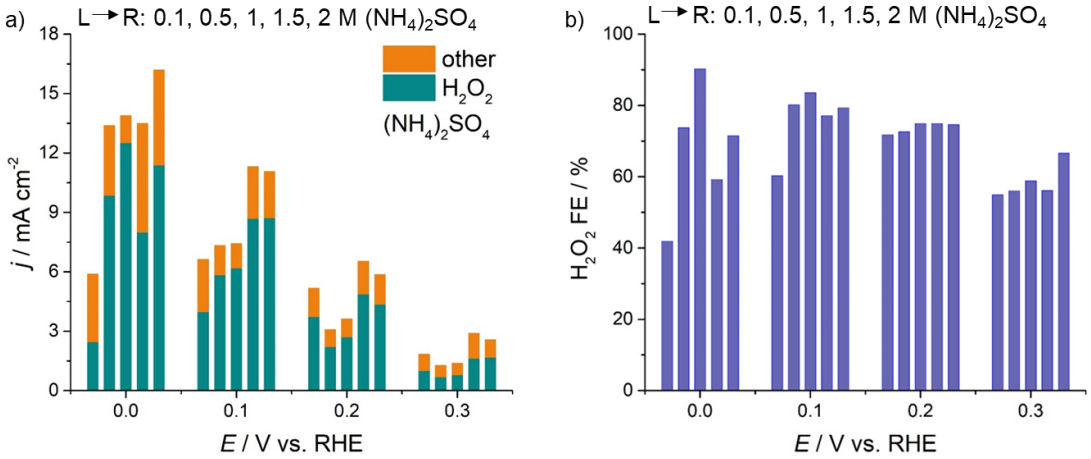

Figure S6. (a) Current density of H_2O_2 and side reaction in O_2-saturated 0.1, 0.5, 1, 1.5, 2 M $(NH_4)_2SO_4$. (b) The H_2O_2 Faraday efficiency in O_2-saturated 0.1, 0.5, 1, 1.5, 2 M $(NH_4)_2SO_4$.

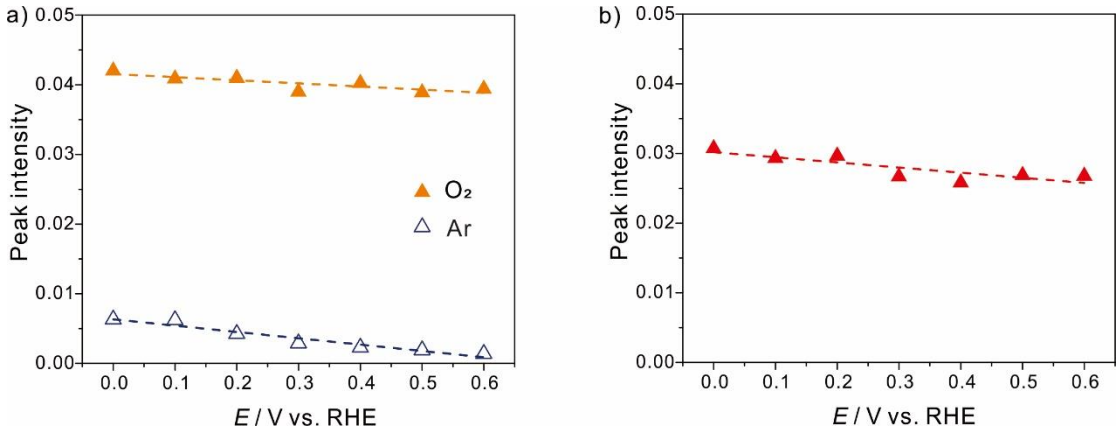

Figure S7. (a) ν(H_2O) peak intensity in Ar and O_2-saturated 1 M Na_2SO_4. (b) ν_3(HOO) peak intensity in O_2-saturated 1 M $(NH_4)_2SO_4$.